NURETH14-249

SIMULATION OF BUBBLY FLOW IN VERTICAL PIPES BY COUPLING LAGRANGIAN AND EULERIAN MODELS WITH 3D RANDOM WALKS MODELS: VALIDATION WITH EXPERIMENTAL DATA USING MULTI-SENSOR CONDUCTIVITY PROBES AND LASER DOPPLER ANEMOMETRY

José L. Muñoz-Cobo^a, Sergio Chiva^b, Mohamed Ali Abd El Aziz Essa^a, Santos Mendes^c

- ^a Instituto de Ingeniería Energética, Universidad Politécnica de Valencia, Valencia, Spain
- ^b Department of Mechanical Engineering and Construction, Universitat Jaume I ,Castellón, Spain

Abstract.

A set of air-water experiments have been performed under isothermal upward concurrent flow in a vertical column. The interfacial velocity, interfacial area of the bubbles and the void fraction distributions was obtained. Numerical validation of these results for bubbly flow conditions were performed by coupling a Lagrangian code which tracks the 3D motion of the individual bubbles, with an Eulerian one. Both Lagrangian and Eulerian calculations were performed in parallel and iterative self-consistent method was developed. The bubbles-induced turbulence is an important issue considered, to obtain good predictions of experimental results.

Introduction

In order to have good predictions of the bubble's motion inside the reactor channels it is required the correct description of the interactions between the dispersed and the continuous phases [1]. Many experimental measurements, and numerical simulations have been performed in recent years to better understand the bubble behaviour in vertical gas-liquid flows [1], [2], [3], [4], and [5]. A better knowledge of the different forces that act on the bubbles moving in a continuous turbulent random fluid field is of importance for a complete description of the bubble's motion and to obtain for instance the radial and axial void fraction distribution, and the gas phase velocity profiles inside the reactor channels [6]. A set of upward co-current air-water flow experiments in a vertical pipe of 52 mm internal diameter was performed at Universidad Politécnica de Valencia (Spain). Local measurements of void fraction, interfacial area concentration (IAC), interfacial velocity and Sauter mean diameter were measured using a four sensor conductivity probe. Numerical simulations of these experiments for bubbly flow conditions were performed by coupling a Lagrangian code, that tracks the 3D motion of the individual bubbles (r,ϕ,z) , to an Eulerian model In a semi two way coupling manner. The velocity and turbulence fields of the liquid phase were computed by solving the time dependent mass, and momentum conservation equations in its Reynolds Averaged Transport Equation form (RANS). The turbulent kinetic energy k, and the dissipation rate ε transport equations were simultaneously solved by using the k, epsilon model in a (r,z) structured grid by the finite volume method using the SIMPLER algorithm. The Hybrid differencing scheme was used for

^c Facultad de Ingeniería Mecánica y Eléctrica, Universidad Autónoma de Nuevo León, Mexico

modelling the convective terms, and the TDMA method was used for solving discretized equations with maximum residual of 1E-4.

1. The Lagrangian model for tracking the bubbles

1.1 The forces acting on a single bubble

The bubble motion in cylindrical coordinates (r, θ, z) in the fluid field is governed by the Newton's second law of motion which is governed by the following set of equations:

$$2?+2???(2-2-2)?=2??,2$$

$$2?+2???(2-2-2)?=2??,2$$

$$(2)$$

$$22+222222=222,2$$
 (3)

Where C_v is the coefficient of the virtual mass force which is assumed equal to 0.5, V_b is the volume of the bubble and $F_{i,r}, F_{i,\theta}, F_{i,z}$ are the radial, azimuthal and axial components of the i-th force acting on the bubble respectively, and the point on the coordinate components means derivation with respect to the time.

The main forces that act on the bubble are the buoyancy force, the drag force, the lift force, the wall-lubrication force and the deformation force. The buoyancy force acting on the bubble is directed in the positive axial direction and its components are given by:

$$222=0, 222=0, 222=22(22-22)2$$
 (4)

The Drag force \vec{F}_{Drag} taken the formula presented by [7]. The next force is the lift force \vec{F}_{LF} , due to the motion of a particle in a fluid field with a velocity gradient in the lateral direction to the main axial motion. This lift force is given according to by the following expression:

$$222 = -2222(22 - 22) \times 2$$
 (5)

Where $\ \ \, \square \ \ \,$ is the bubble velocity, $\ \ \, \square \ \ \,$ is the liquid velocity, $\ \ \, \vec{\omega}$ is the vorticity of the liquid velocity field, and $\ \ \,$ C $_T$ is the Tomiyama lift force coefficient, [8], The vorticity in cylindrical coordinates is computed by means of the expression:

Because the CFD calculations shows that the velocity profile is logarithmic, we have assumed that the average fluid velocity profile in the z direction that is being used to compute the vorticity depends on the radial coordinate in the developed flow region. Then, the lift force inside a pipe can be computed by means of the following expression:

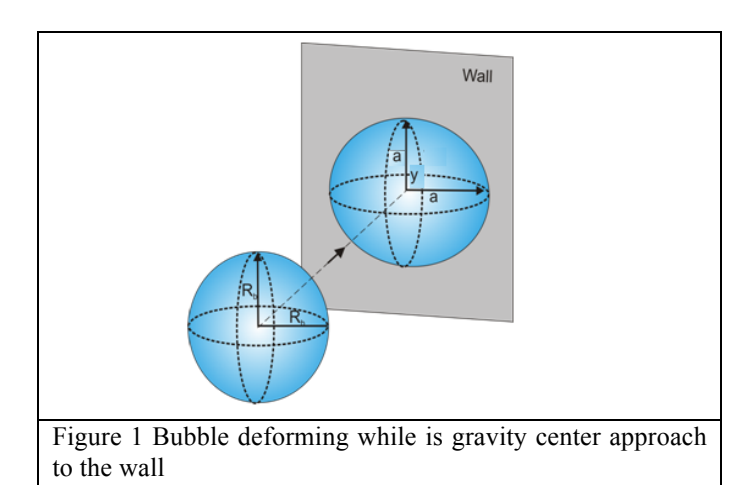
The next force considered in the model is the bubble deformation force. According to [1]. To compute this force we have assumed a bubble that when approaching and touching the walls deforms and adopts an oblate shape as displayed at figure 1. After some mathematical manipulations described in details in [9] the final form of this force will be as follows:

$$2222 = -\partial 2(2) \quad \partial 222 = 22 \quad 222222222222$$
 (8)

where we have defined the following function that depends only on R_b/y , because μ' depends also on R_b/y

$$?=?2?2-10.5=??3?3-10.3$$
 (9)

This deformation force \vec{F}_{Def} is directed toward the centre of the tube and after the bubble compression can provoke the bouncing of the bubble as showed in Zaruba et al experiments [1].



The last force considered is the wall lubrication force. At the wall, the drainage rate between the bubble and the wall is slower than the other side due to wall non-slip condition. As a result, the bubble suffers a hydrodynamic force known as wall lubrication force. The expression for this force was first deduced by [10], and then improved by [4]:

The coefficient in [8] for the wall lubrication force is given in terms of the bubble Reynolds number Re_b and the Eotvos bubble number, Eo_b, And the function $f_{wL}(r)$, that defines the wall lubrication forces near the wall are expressed as follows:

$$222=222$$
 $7221.9,0.021722$ 2 $222=2212-2$ $2-12+2$ 2 (12)

being R the tube radius and d_b the sphere equivalent radius of the bubble, Re_b and Eo_b are the Reynolds and the Eötvos numbers respectively for the bubble given by:

$$222 = 222 - 22222$$
, $222 = 2(22 - 22)222$ (13)

1.2 The model of turbulent diffusion by eddies and the connection with the CFD model for the continuous phase.

In this work, the time-averaged velocity and the turbulence properties are calculated by solving the RANS Navier-Stocks equations, and the k- ϵ turbulence model, to build a statistical model that gives the instantaneous fluid fluctuation velocities that are seen by the bubbles in a Lagrangian frame. However, we must take also into account the turbulence induced by the bubbles.

The liquid velocity $\vec{u}_l = \vec{u}_l + \vec{u}_l'$ that appears in equations (5), and (11) is composed of an average part \vec{u}_l that is computed solving the RANS equations and a fluctuating part \vec{u}_l' due to the eddies that is obtained by a continuous random walk model in 3D, with isotropic turbulence, that in the region where the flow is completely developed we have assumed obeys the following Langevin equation:

$$22222=-22222$$
, 2222 , 2222 , 2322 2322 2322 2322 2322 2322

Where k(r,z) denotes the turbulent kinetic energy at point (r,z),. We have assumed to simplify the calculations, that there is not azimuthal dependency by the symmetry of the problem. τ_L is the characteristic time of the Lagrangian time scale correlation (see [11] for details). Finally the vector $\vec{\xi}(\xi_r, \xi_\theta, \xi_z)$ denotes a Gaussian vector white noise random process, with components that are independent Gaussian random numbers.

The model given by equation (14) assumes isotropic turbulence. The characteristic time τ_L is computed away from the boundary layer by the following expression:

$$222,2 = 0.142(2,2) \qquad 2(2,2) \qquad 2 + = (2-2) \qquad 2 + 22 > 100 \qquad (15)$$

At the boundary layer we have used the following expression computed by DNS by [12]:

Where the non-dimensional Lagrangian time scale is defined by $\tau_L^+ = \tau_L \frac{(u^*)^2}{v_L}$.

Equation (13) is equivalent to the following stochastic differential equation system:

$$2?? = -?????,?$$
 $?? + 2???,?$ $122?$ $?,?$ $3?$ $?$ (17)

Where $d\vec{W}$ is a 3 dimensional Wiener process.

In order to compute the turbulence kinetic energy, we must also consider the turbulence induced by the bubbles in the liquid phase. We have assumed particulary that the turbulence kinetic energy induced by the bubbles depends on the void fraction and the Reynolds number for the bubbles, so we considered the total turbulence kinetic energy as:

$$2=22+22$$
 , $22=2222$ 222 (18)

Where k_b introduces the turbulence induced by the bubbles. The value of C_{1b} has been chosen equal to 5.5E-, this value provide good results for the experiments performed at a liquid velocity of 2m/s, as we will display later. However if we have assumed that 22 depends also on the gradient of the void fraction we may write:

$$2?? = 2??1 + 2??2\nabla?$$
 (19)

Where C_{Ib1} =2.0E-5, and C_{Ib2} =5.5E-5 by fine tuning with experimental results. These values provided good results for the experiments performed at 2 and 3 m/s.

When the bubbles move in the axial direction inside the pipe they expand its size because the pressure exerted by the liquid column diminishes. This expansion is taken in account in our code considering the air inside bubbles behaves like a perfect gas.

4 EXPERIMENTAL FACILITY, INSTRUMENTATION AND EXPERIMENTS

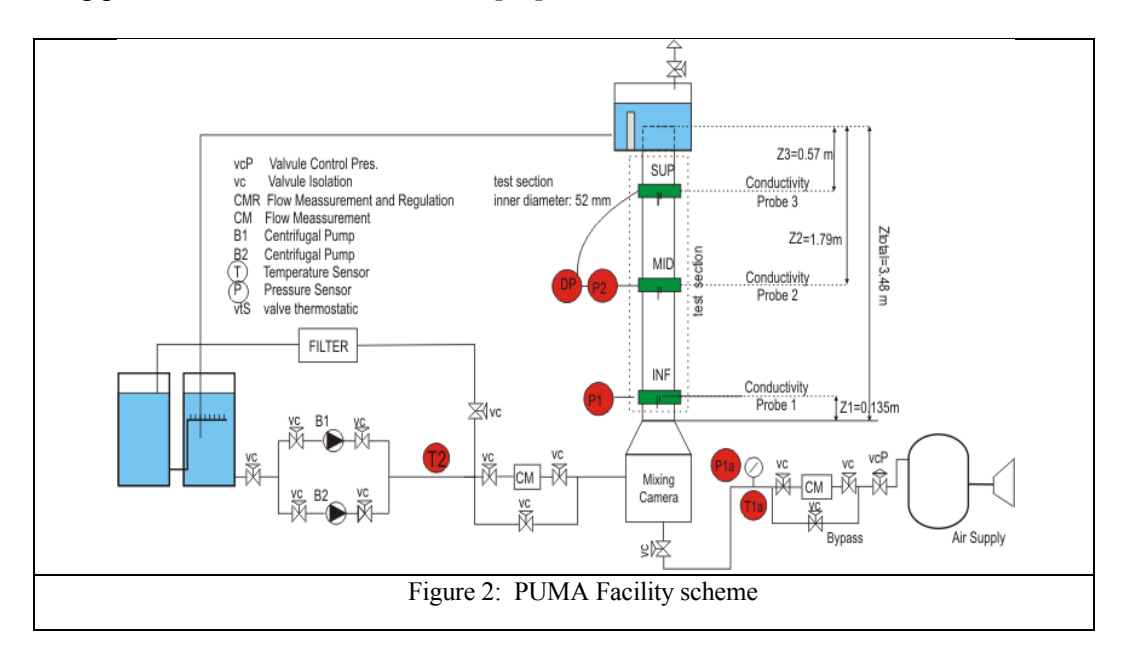
4.1 Description of the experiments

The experimental facility used to perform the experimental work is schematically illustrated in Figure 2. The test section is a round transparent tube of Plexiglas® with inner diameter of 52mm and height of 3340 mm. The air is supplied by an air compressor and it is introduced to the test section through a porous sinter element with an average pore size of 40µm installed below the mix chamber at the lower plenum. The air and water Temperature is kept constant during the test essay. More details of the experiments performed and instrumentation can be found in [9] and [13]. The experiments used for comparison in this work have the conditions as illustrated in table (1).

$j_f = 2.0 \text{ m/s}$			$j_{\rm f} = 3.0 \; {\rm m/s}$		
_	j_g [m/s]	<a>[%]		j_g [m/s]	<α>[%]
F03G01	0.209	3.69	F04G01	0.363	5.04
F03G02	0.231	8.18	F04G02	0.407	9.76
F03G03	0.268	14 90			

Table 1 Experimental Flow Conditions

Hint: the same experiments were made using four point probe to measure void fractions. the difference between F03G02, and F03AG02 is that they were made with different configurations of the measuring probe as described in details in [12].



3 Computational results and comparison with some experiments

The dispersed phase is computed by tracking the bubbles along its trajectories. The bubbles are generated with a uniform distribution at the bottom of the pipe, the diameter of the bubbles is sampled uniformly in the interval [2.1mm,2.9mm] according to the experimental data for the Sauter Mean Diameter and collected in the top level of the pipe. The total number of bubbles tracked to compute the void fraction distribution is twenty thousand (20,000).

The computational process is made a semi two way coupling algorithm in the following order; we start with the liquid turbulence alone in the continuous random walk model (CRW), then solving the RANS equations for the continuous phase and the Lagrangian model for the bubbles. We obtain a first iterated value for the void fraction distribution that is more peaked than the experimental one, because it does not take into account the random walk diffusion induced by the bubbles themselves. This distribution is used as an input to integrate the Lagrangian equations again, and in this way we obtain a second iterated value of the void fraction distribution. After three or four iterations the void fraction distribution converges and gives values that are close to the experimental ones.

The predictions of the void fraction distribution is very good in all the points as shown in figures 12 to 21. The maximum position of the void fraction distribution and its value are also well predicted by the Eulerian-Lagrangian model developed in this paper. The point near the wall has been computed a little bit near the wall than the experimental value. However it seems that the experimental value is higher than the computed one. This difference is due to the bubbles with diameters smaller than 2.1 mm. that slides over the liquid film close to the wall.

When the average void fraction increase to $<\alpha>=0.1490$ as in run F03G03 and the superficial velocity of the liquid phase is maintained in j_f =2 m/s, then the predictions obtained using equation (18) for the turbulence induced by the bubbles, with $C_{Ib} = C_{Ib0} = 5.5 \times 10^{-5}$ match the void fraction peak position, and the void fraction distribution in the middle region but the experimental peak is broader than the calculated one as observed in figure 14. When we try to make predictions of the cases with higher liquid superficial velocities we achieve good predictions for all the cases if we consider that C_{Ib} in equation (18) depends on the void fraction gradient as in equation (19), 222=221+2222, this assumption makes the wall peak broader as displayed at figure 14.

The calculated results are displayed with open circles and line in the gap and the experimental one with red solid circles. We notice that the predicted height of the wall peak is a little bit bigger than the experimental one. For higher velocity values the model predict well the fact that the height of the wall peak diminish when the superficial liquid velocity increases as displayed in figures 15 and 16 for Runs F04G01 and F04G02. The gas velocity for different radial positions was averaged for all the range of bubbles at this position in order to be able to compare with the experimental results. This profile matches quite well with the experimental one, as is showed at figure 17.

One of the most important parameter to be calculated in the two-phase flow simulations is the Interfacial Area Concentration IAC. Most of the code use a simplified model based on spherical monodispersed bubble, and only codes that use population balance approach or similar expensive technique are able to give good predictions but restricted to bubbly regimen. In our model we have calculated the interfacial area concentration taking on account the contribution of interfacial area of all the individual bubbles. As shown in figures 18 to 21, we can observe that the

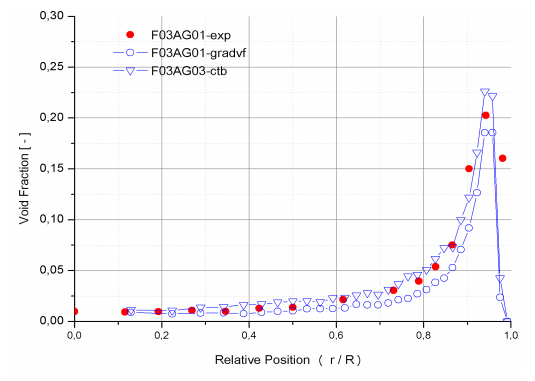


Figure 12 Void fraction versus r/R for case F03G01, The solid circles denote the experimental results, while the open circles are the calculated results with CIb=CIb1+CIb2Vα, and the triangles with CIb=CIb0

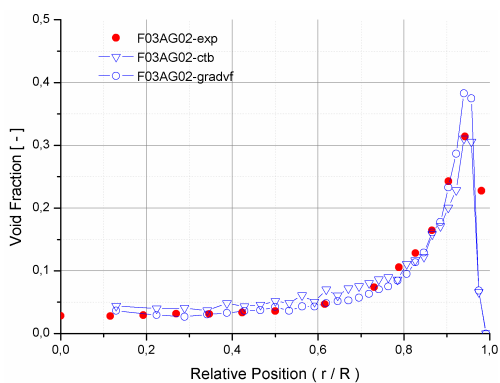


Figure 13 Void fraction versus r/R for case F03G02, The solid circles denote the experimental results, while the open circles are the calculated results with Clb=Clb1+Clb2 $\nabla \alpha$, and the triangles with Clb=Clb0

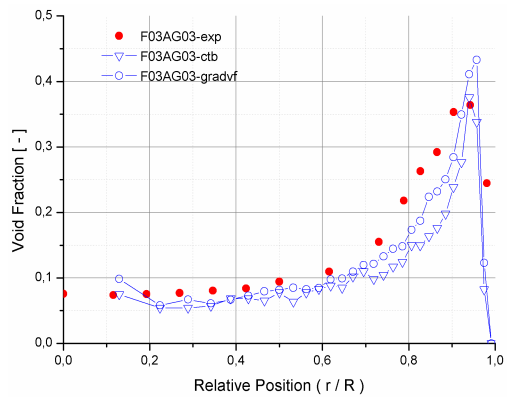


Figure 14. Void Fraction Profile for Run F03G03, The solid circles denote the experimental results, while the open circles are the calculated results with CIb=CIb1+CIb2 $\nabla\alpha$, and the triangles with CIb=CIb0

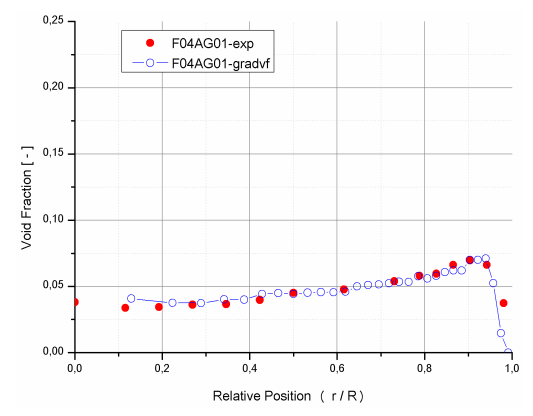


Figure 15. Void Fraction Profile for Run F04G01, the solid circles denote the experimental results while the open circles are the calculated values with $CIb=CIb1+CIb2\nabla\alpha$

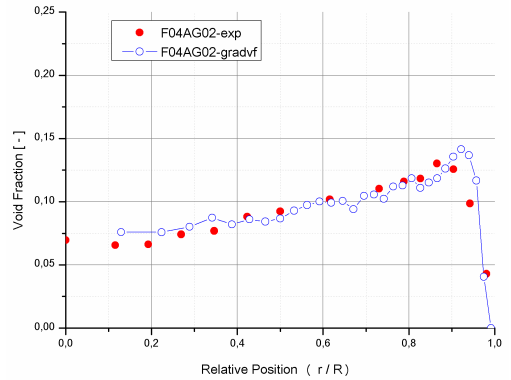


Figure 16. Void Fraction Profile. Run F04G02, Solid Circle: experimental results, Open Circle: CIb=CIb1+CIb2 $\nabla \alpha$

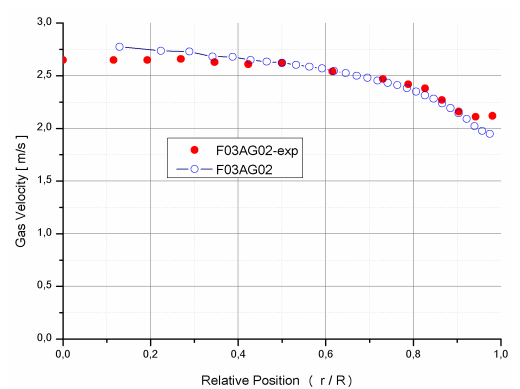


Figure 17. Interfacial area velocity profile for Run F03G02, The solid circles are the experimental results. The open circles are the calculated results with vf gradient:

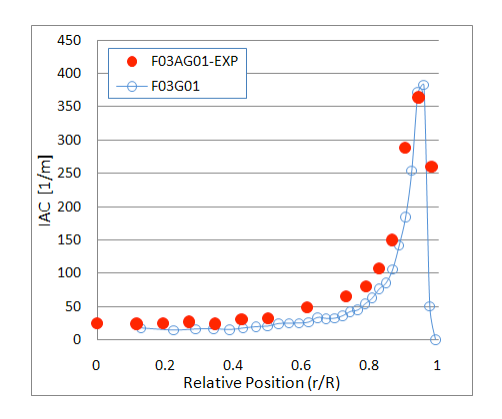


Figure 18. Interfacial area concentration (IAC) for Run F03AG01

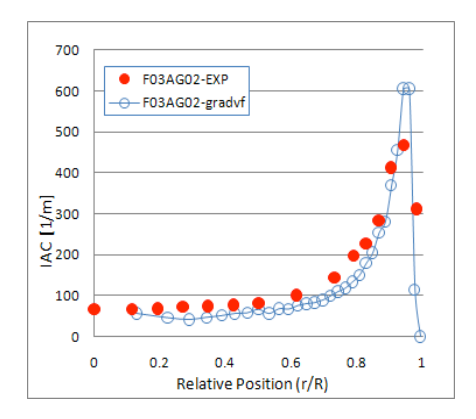


Figure 19. Interfacial area concentration (IAC) for the Run F03AG02

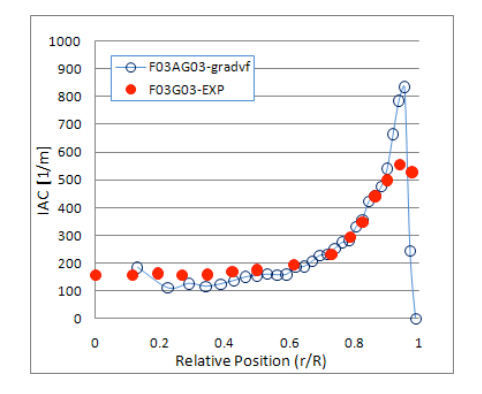


Figure 20. Interfacial area concentration (IAC) for Run F03AG03

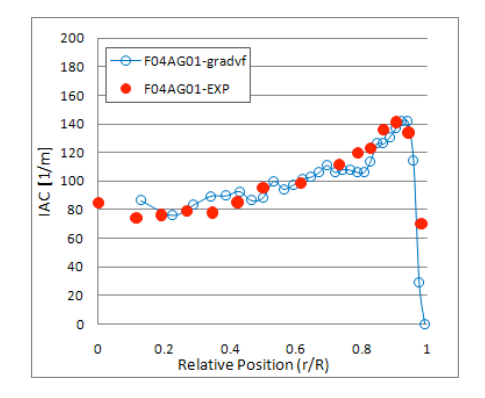


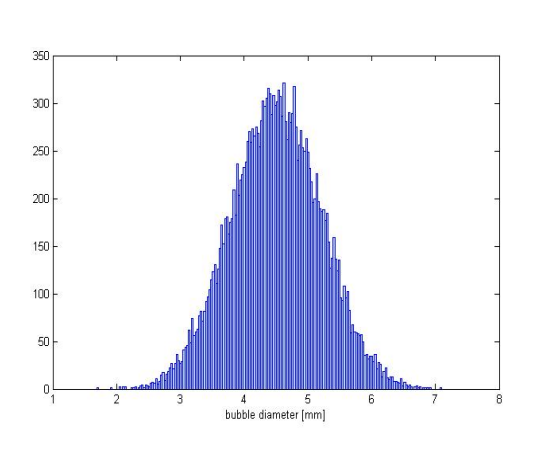
Figure 21. Interfacial area concentration (IAC) for Run F04AG01

calculated results give a very good agreement with the experimental ones, especially for the cases F03G01 and F04G01. The higher peak values can be explained by the prediction of the higher values of void fraction at this radial zone, as it has been commented in the previous paragraphs, and mainly due to the presence of more bubbles with little diameter ranges than that used in calculation.

We have tested the code for the ability of working in a large range of bubble diameters and how will be distributed each group of bubble diameters. We have generated a Gaussian distributed bubble diameters ranging from 2 mm up to 7 mm, which have a histogram distribution as shown in figure 23.

We have divided the bubble diameters to eight groups of diameters to show the ability of the program to treat each group depending on the range of diameters. As we can see in figure 24, the total void fraction distribution, solid black line, is shown for the presented range of diameters, and or each group the void fraction profile has been graphed. The smallest bubble diameters migrate in the direction of the wall, this can be observed by the peak of void fraction near the wall up to D_{bub} =5.8mm. For D_{bub} >5.8mm the largest diameters migrate in the direction

of the tube centre and the wall peak disappears. This behaviour gives agreement with experiments of bubble diameter grouping performed by [14] using wire mesh.



--- Dh<3.5 mm ____ 3 5 mm<Dh<4 mm ____ 4 mm<Dh<4 5 mm -4.5 mm<Dh<5 mm _____5 mm<Dh<5 5 mm - 6 mm<Db<6.5 mm → Db> 6.5mm total Void fraction 0.65 0.05 0.6 0.55 Void Fraction Percent 0.5 0.45 0.4 0.35 0.02 0.3 0.25 0.15 0.1 0.05 0 ' -0.01 0.90 0.00 0.10 0.20 0.30 0.40 0.50 0.60 0.70 0.80 1.00 Relative Position (r/R)

Figure 23. Gaussian bubble diameter histogram generated

Figure 24. The distribution of void fraction for different bubble diameter ranges represented as a percent of the total void fraction of a on the left y axis, and the total void fraction on the right y axis

4 Conclusions and Future Developments

The Eulerian-Lagrangian model with a 3D random walk model developed in this paper gives good prediction of the void fraction distribution for bubbly flow cases. The turbulence induced by the bubbles plays an important role in the continuous random walk model because when this mechanism for turbulence production is not included, then the peak for the void fraction profile is higher than the experimental one. Since the void fraction distribution is not known a priori then a self-consistent calculation is performed in order to obtain the void fraction distribution. This is achieved by executing a set of iterations to obtain the true void fraction profile. The first void fraction distribution is obtained considering only the liquid turbulence. The output of this calculation is a first iterated void fraction distribution that is used as input for the second calculation and so on. The convergence is achieved in three or four iterations.

Another important thing is that to compute the turbulence induced by eddies given by equation (18), the model predictions improved when we assume that the constant C_{Ib} that appears in equation (18) is assumed to depend on the gradient of the void fraction profile as written in equation (19). Good predictions of the void fraction distributions are obtained for the cases with liquid superficial velocities of 2 and 3 m/s, and also for the interfacial velocity distributions. The interfacial area concentration has been predicted with a very good agreement with the experimental results.

However this model does not included the coalescence of the bubbles, or the break up of the bubbles by interactions with turbulent eddies. So the next step is to include in this Eulerian-

Lagrangian model the Break-Up and Coalescence mechanisms in order to go to the cap/slug regime. In this way we could make predictions of the void fraction distribution for several group of bubbles. The model is being improved by including these interaction mechanisms in a full Lagrangian-Eulerian model were group of bubbles are simultaneously tracked.

5 Acknowledgments

The authors of this paper are indebted to the National Plant of I+D by the support of the coordinated projects EXPERTISER ENE2007-68085-C02-01/CON and EXPERTISER ENE2007-68085-C02-02/CON to perform the experiments.

6 REFERENCES

- [1]. Zaruba, D. Lucas, H. M. Prasser, and T. Höhne"Bubble-wall interaction in a vertical gasliquid flow: Bouncing, sliding and bubble deformations", Chemical Engineering Science, Vol. 62, 2007,pp. 1591-1605.
- [2]. Zun, I. Kljenak, and S. Moze, "Space-time evolution of the non-homogeneous bubble distribution in upward flow". Int. J. Multiphase Flow, Vol. 19, 1993, No. 1, pp. 151-172.
- [3]. H.M. Prasser, E. Krepper, and D. Lucas "Evolution of the two phase flow in a vertical tube, decomposition of gas fraction profiles according to bubble size classes using wire-mesh sensors". International Journal of Thermal Science, Vol. 41, 2002, pp. 17-28.
- [4]. Tomiyama, I. Zun, H. Higaki, Y. Makino, and T. Sakaguchi, "A three dimensional particle tracking method for bubbly flow simulation", Nuclear Engineering and Design, Vol. 175, 1997, pp. 77-86.
- [5]. D. Lucas, E. Krepper, and H.M. Prasser, "Development of co-current air-water flow in a vertical pipe". International Journal of Multiphase Flow, Vol. 31, 2005, pp. 1304-1328.
- [6]. E. Krepper, D. Lucas, H.M. Prasser, "On the modelling of bubbly flow in vertical pipes". Nucl. Eng. Des, Vol. 235, 2005, pp. 597-611.
- [7]. Tomiyama, "Struggle with computational Dynamics". <u>Third International Conference on Multiphase Flow</u>. ICMF 98. Lyon. France. 1998,
- [8]. Tomiyama, H. Tamai, I. Zun, and S. Hosokawa, "Tranverse migration of single bubbles in simple shear flows", Chemical Engineering Science, Vol. 57, 2002, pp.1849-1858.
- [9]. J.L. Muñoz-Cobo, S. Chiva, S. Mendez, M. A. Abdelaziz, "Coupled lagrangian and eulerian simulation of bubbly flows in vertical pipes: validation with experimental data using multi-

- The 14th International Topical Meeting on Nuclear Reactor Thermal hydraulics, NURETH-14 Toronto, Ontario, Canada, September 25-30, 2011
 - sensor conductivity probes and laser doppler anemometry ", <u>CFD4NRS-3 Workshop</u>, Bethesda north marriott Hotel &Conference Centre, Bethesda , MD,USA, 14-16 September 2010.
- [10]. S.P. Antal, R.T. Lahey Jr and J.E. Flaherty, "Analysis of two phase flow distribution in fully developed laminar bubbly two-phase flow", Int. J.Multiphase Flow, Vol. 17,No. 5, 1991,pp. 635-652.
- [11]. Dehbi, "Turbulent particle dispersion in arbitrary wall-bounded geometries: a coupled CFD-Langevin-equation based approach", Int. J.Multiphase Flow, Vol. 34, 2008, pp.819-828
- [12]. G.A. Kallio, and Reeks, M.W., "A numerical simulation of particle deposition in turbulent boundary layers". Int. J. Multiphase Flow, Vol. 3, 1989, pp. 433-446.
- [13]. Santos Mendez Diaz, "Medida Experimental De La Concentración De Area Interfacial", PhD Thesis, 2008, Universidad Politécnica de Valencia, Spain,
- [14]. H.M. Prasser, M. Beyer, H. Carl, S. Gregor, D. Lucas, H. Pietruske, P. Schütz, and F.P. Weiss, "Evolution of the structure of a gas-liquid two-phase flow in a large vertical pipe". Nuclear Engineering and Design, Vol. 237, 2007,pp. 1848–1861.
- [15]. B.E. Launder, B. Spalding,1972, "Mathematical Models of Turbulence". Academic Press, New York.
- [16]. J.L. Muñoz-Cobo, J. Peña, S. Chiva, S. Mendez, "Monte-Carlo calculation of the calibration factors for the interfacial area concentration and the velocity of the bubbles for double sensor conductivity probe", Nuclear Engineering and Design, Vol. 237, 2006,No. 5, pp. 484-496.
- [17]. T.L. Bocksell, E. Loth, , "Stochastic modelling of particle diffusion in a turbulent boundary layer", Int. J. Multiphase Flow, Vol 32, 2006, pp.1234-1253
- [18]. T.R. Auton, "the lift force on a spherical body in a rotational flow", Journal of Fluid Mechanics, Vol 183, 1987, pp.199-218